

Fermion Loops, Linear Magnetoresistance, Linear In Temperature Resistance, and Bad Metals

Vincent Sacksteder IV*

*Department of Physics, Royal Holloway University of London,
Egham Hill, Egham, TW20 0EX, United Kingdom*

Bad metals including the high T_c superconductors display an exotic resistance that is linear in both temperature and magnetic field. This hallmark of strong correlations is poorly understood. We show that Fourier transforming the magnetoconductance with respect to magnetic field obtains a curve describing the area distribution of loops traced by electrons and holes within the sample. Analysis of this area distribution reveals that linear resistance is caused by scattering and quantum interference, but with more large loops than occur in ordinary 2-D and 3-D materials where scattering destroys quantum coherence and limits loop size. This limit on quantum coherence is absent in linear resistance materials, resulting in larger loops limited only by thermal decoherence. Linear resistance signals that quantum coherence is maintained in the presence of scattering.

PACS numbers: 72.15.Rn,73.23.-b,71.27.+a,74.72.Kf

In atomic units $m_e = e = \hbar = k_B = 1$ the magnetic field B has dimensions of inverse area, which is key to understanding the electrical conductance's dependence on B . Large fields probe areas at the scale of the unit cell, and small changes in field probe much larger areas. At large fields one finds Landau levels and Schubnikov-de Haas (SdH) oscillations, which are visible in the longitudinal conductance $G_{xx}(B)$ as peaks at characteristic field strengths determined by the Fermi energy E_F . The Fermi surface's cross section, an inverse area, can be read off from the peak positions. Landau levels and SdH oscillations are signals of ballistic physics, i.e. weak scattering, and are extinguished once scattering becomes too frequent.

At small fields one finds weak (anti) localization (WL/WAL), where scattering and quantum interference cooperate to cause G_{xx} to decrease or increase with field depending on whether spin rotation symmetry is broken faster or slower than time reversal symmetry. WL/WAL contrasts strongly against Landau levels and SdH oscillations. It is much more sensitive to magnetic field, is visible at much smaller field strengths, and varies smoothly with field rather than exhibiting oscillations. Moreover WL/WAL requires scattering and is weakly sensitive to length scales shorter than the scattering length, including the atomic unit cell and the Fermi wavelength.

Recent years have exposed mysteries which lie well beyond traditional SdH and WL/WAL physics. Many experiments report systems where the longitudinal resistance R_{xx} increases linearly with B and does not saturate.^{1–11} This contrasts both with SdH oscillations which oscillate periodically in $1/B$ and with WL/WAL which is logarithmic. Explanations have been given for the cases of ballistic conduction when the Fermi surface has a cusp, of a 3-D Dirac cone in the presence of a strong magnetic field, of a density gradient across the sample, and of classical transport with strong sample inhomogeneities.^{12–16} However this kind of case by case treatment is not entirely satisfactory given the wide range of experimental realizations.

Another long-standing mystery is that high T_c superconductors (cuprates and pnictides) at temperatures above the superconducting phase display a resistance which increases linearly with temperature and does not saturate.¹⁷ This is inconsistent both with the WAL signal which increases much more slowly with T (logarithmically in 2-D and as a square root in 3-D) and with phonon based scattering which should saturate at a maximum determined by the atomic spacing. Materials whose resistance is linear in temperature are called bad metals and are understood to be strongly correlated, but the details of the conduction process responsible for linear resistance are not understood. It is widely believed that linear-in-temperature resistance is correlated with high- T_c superconductivity. Very recently the linear dependence on temperature has been linked to linear magnetoresistance found in the same bad metal regime.^{18–20}

This paper, inspired by the magnetic field's units, develops a geometrical analysis of magnetotransport in terms of the loops traced by electrons and holes as they move through real space, magnetic fluxes through those loops, and the Aharonov-Bohm effect. The starting point of our analysis is Feynman's formulation of quantum mechanics as a sum over paths.²¹ In this formulation an electron follows not just one path, but instead many paths which fully explore the sample in which the electron is moving. All of these many paths are summed to determine the evolution of $|\psi\rangle$, the electronic state. In this paper our focus is not on the state $|\psi\rangle$, but on the many paths that contribute to $|\psi\rangle$. The two pictures are mathematically equivalent: starting from a knowledge of paths one can build the electronic propagator which controls the evolution of $|\psi\rangle$, and conversely $|\psi\rangle$'s evolution may be systematically decomposed into the paths which determine it.

To be clear, we are not discussing the semiclassical paths of an electron's average motion. For instance, in a magnetic field an electron's average position executes well-defined circular loops around the axis of the magnetic field, and one can measure this cyclotron motion.

This is not the sort of path we are talking about. Instead we are talking about the infinitely many quantum mechanical paths, tracing many complex trajectories and fully exploring the sample, which sum up to produce the average cyclotron motion.

The paths traced by electrons never begin or end in isolation, since in this event electronic charge would not be conserved, i.e. charge would be generated or destroyed. Instead, the creation or annihilation of an electron is always accompanied by the creation or annihilation of an accompanying hole with opposite charge, and by this mechanism charge is conserved. The two paths of an electron and of its corresponding hole, followed from their origin together to their final disappearance together, form a loop.

It is important to be clear that the loops under discussion here are traced by bare electrons and holes, not by quasiparticles. The requirement to move in loops is an immediate consequence of charge conservation and gauge invariance, and does not require that interactions are weak, the existence of a Fermi liquid, or well-defined quasiparticles, and does not assume any other sort of collective many-body behavior. The loop requirement applies independently of magnetic fields, scattering, and interactions. Analysis focused on electron-hole loops is therefore a very powerful way of understanding the mechanisms responsible for electronic transport.

It is also important to be clear that the loops discussed here move through real space, and occur even when disorder is very strong. Therefore they are not the same loops used in the analysis of Berry phases and topological invariants, which are usually calculated in momentum space and assume a well defined band structure. Moreover the loops discussed here concern the bare electron and hole carriers within a material; the U(1) symmetry which supports them comes from electromagnetism, not from effective interactions that occur in spin liquids and other interacting systems.

Experimental data on a sample's magnetic field dependence gives direct access to the areas of the electron and hole loops within the sample. Each loop couples to field via a phase which is proportional to the magnetic flux through the loop, and this phase is equal to the product of the loop area and the magnetic field strength. There is also a Zeeman term, which we neglect for the moment and will return to later. Within the phase factor magnetic field has a conjugate relationship to area, with a proportionality constant that is determined by fundamental constants and can not be renormalized. Therefore measurements of a sample's magnetic field dependence allow rigorous conclusions to be made about the areas of the loops traced by electrons within the sample, and give a window onto the physical processes and length scales at work in transport. The methodology of using magnetic fields to measure loops, which we explain further below, does not assume quasiparticle or Fermi liquid physics. It is a simple consequence of charge conservation.

In this article we apply this methodology to electrical

conduction and obtain rigorous results about the electron and hole loops responsible for Landau levels, SdH oscillations, WL/WAL, and linear magnetoresistance. Our rigor here is founded on the firm link between experimental observables and loop areas, and does not concern details of the material's Hamiltonian, interactions, Fermi surfaces, or disorder. In fact these points are discussed very little here. Instead we focus on reasoning about the electron and hole loops that are responsible for conduction, and on drawing conclusions about which physical mechanisms are responsible for producing them.

First we focus on scattering. The electron loops responsible for Landau levels and SdH oscillations, which are phenomena that do not rely on scattering, have weights that oscillate periodically with loop area, and the period of oscillation is determined by the Fermi surface. In contrast, the weights of the loops responsible for the WL/WAL signal decrease gradually and smoothly with area, and the decay extends to loop areas which are far larger than that determined by the Fermi surface. The very smooth distribution of loop areas and the very large area scales are caused by stochastic motion of the charge carriers, and are unmistakeable hallmarks of scattering. Moving on to linear magnetoresistance, in this case the loop areas again decrease smoothly up to very large areas. These results are mathematically rigorous, and are conclusive evidence that scattering is key to linear magnetoresistance.

The weights governing loop areas for WL/WAL²²⁻²⁴ and for linear magnetoresistance show two additional similarities: both do not show any concentration near any particular area scale (i.e. both are scale-free), and both have a single sign. In our view the root cause of linear magnetoresistance is the same interplay of scattering and quantum coherence that causes WL/WAL in standard Fermi liquids. In standard WL/WAL scattering is caused by static impurities, and in bad metals scattering is caused by electronic interactions, but in both cases the effects of scattering on electronic conduction are broadly the same. First of all, at lengths exceeding the scattering length l the electronic wave-function $|\psi\rangle$'s phase is randomized, rendering single wave-functions unable to mediate conduction. Therefore conduction over distances longer than l is mediated only by pairing between $|\psi\rangle$ and its complex conjugate $\langle\psi|$, whose random phases cancel. This pairing produces the single-particle density matrix $\rho(x)$, which is the key mediator of conduction at distances longer than the scattering length. This result is well known from the extensive work on sigma models and bosonization techniques in disordered systems.^{23,25}

ρ 's evolution is sensitive only to processes where $|\psi\rangle$ and $\langle\psi|$ undergo the same scattering events and follow the same path between scatterings, because only these processes satisfy the requirement that the disorder-induced random phases of $|\psi\rangle$ and $\langle\psi|$ must cancel. There are two such processes, the diffuson and the Cooperon. In the diffuson $|\psi\rangle$ and $\langle\psi|$ follow the same sequence in the same order, producing purely classical electronic motion.

In the Cooperon $|\psi\rangle$ and $\langle\psi|$ follow the same sequence but in reversed order, and their phases seem to be randomized with respect to each other. It is not until their trajectories close a loop and come back to their origin that $|\psi\rangle$ and $\langle\psi|$'s phases suddenly cancel and $\rho(x)$ undergoes a revival. The Cooperon is a quantum interference process, distinct from classical motion, and is strongly dependent on even very weak magnetic fields. It is the Cooperon's contribution to conduction which is responsible for WL/WAL, and which we assert is responsible for linear magnetoresistance.

Our assertion that Cooperons are responsible for linear magnetoresistance should not be read as an assertion that bad metals are governed by impurities, elastic scattering instead of interaction-based scattering, Fermi liquid physics, or quasiparticles. We are simply stating that scattering and stochastic motion are key, and that both WL/WAL and linear magnetoresistance are caused by pairs of matching loops, one for $|\psi\rangle$ and one for $\langle\psi|$, following identical trajectories but in opposite directions. These paired loops are the Cooperon, whose distribution of loop areas is scale free and smooth and extends to very large areas, as seen both in standard WL/WAL and in linear magnetoresistance.

We are making an assertion about the time scale of the interactions responsible for scattering in linear magnetoresistance. These interactions, and the electron-hole loops responsible for them, must fluctuate slowly enough to give Cooperons enough time to close their loops. However the time required to complete a Cooperon loop is very short - later in the text we estimate several picoseconds for Cooperon loops of area $A = (100 \text{ \AA})^2$. As long as the electron and hole loops within the sample fluctuate more slowly than this time scale, they can cause the scattering necessary for Cooperon loops, WL/WAL, and linear magnetoresistance.

Comparison of the loops responsible for standard WL/WAL and for linear magnetoresistance does reveal one important difference between the two: there are many more large loops in linear magnetoresistance than in WL/WAL. This distinction is mathematically rigorous: the probability distribution of WL/WAL's loop areas decays like $1/A$ (A is the area), while the area distribution for linear magnetoresistance decays like $\ln A$; i.e. it has a long tail. We argue that the long tail is caused by quantum coherence, which results in quantum mechanical harmonics. One example of harmonics is the sequence of Landau levels, where the lowest Landau level is accompanied by many siblings whose areas are multiples of the area in real space of the lowest level. In standard WL/WAL scattering randomizes momentum, and therefore each Cooperon loop is not accompanied by harmonics at multiples of its area. This leads directly to the standard WL/WAL signal. If however each Cooperon loop is accompanied by repeats at multiples of its area, then one finds a long tail in the loop area distribution and can obtain linear magnetoresistance. We therefore interpret linear magnetoresistance as unambiguous evi-

dence that the charge carriers maintain their coherence and manifest many harmonics, despite undergoing scattering. In other words, linear magnetoresistance is caused by a combination of quantum coherence and scattering that is not present in ordinary materials. This deduction is based on the long logarithmic tail in the loop areas that are responsible for linear magnetoresistance, which is a rigorous result. It concerns physics at distances much large than the scattering length, and therefore is both agnostic about and independent of microscopic details of the Hamiltonian, interactions, and how quantum coherence is preserved.

Turning now to the linear-in-temperature resistance seen in bad metals, in our view it is nothing other than the zero-field manifestation of linear-in-field resistance. Quantum mechanical harmonics are regulated only by temperature and scattering. In linear magnetoresistance systems the higher harmonics responsible for large loops are resilient against scattering, but not against temperature, and increasing temperature reduces the number of harmonics. The precise mapping from linear in field resistance to linear in temperature resistance is required by a very simple and weighty fact: when the field is reduced to zero, temperature supplies the only area scale comparable to the areas of the very large loops in play in linear magnetoresistance.

Our explanation contrasts with most other work on bad metals, which typically neglect the quantum interference contributions to electronic conduction which are responsible for WL/WAL, and focus on a momentum relaxation time scale τ which varies inversely with temperature and at large temperatures becomes very short, opening up a range of questions about correlation effects at short time scales¹⁷, as well as the puzzling consequence that τ can be smaller than \hbar/E_F , where E_F is the Fermi energy.²⁶ Explanations of linear in temperature resistance have been given using resonating-valence-bond theory²⁷, marginal Fermi liquids²⁸, hydrodynamics of quantum critical liquids²⁹, the SYK model with effective medium theory³⁰, and bounds on diffusion in incoherent metals²⁶. In Refs.²⁷⁻²⁹ the momentum relaxation time $\tau \propto T^{-1}$ scales inversely with temperature, and therefore simple formulas such as the Drude formula which have $\rho \propto \tau^{-1}$ produce in linear in temperature resistance. Quantum interference is omitted from these simple estimates of the resistance. Ref.²⁶ follows a similar argument but instead of τ uses a time scale $\tau_{\text{eff}} \propto T^{-1}$ which controls diffusion. Ref.³⁰ computes the resistance from the leading order term in Boltzmann theory, with a self-energy $\Sigma \propto \tau^{-1}$ which is linear in T . These works all use simplified calculations of resistance which omit quantum interference effects, including WL/WAL and Anderson localization, and lay the responsibility for linear in temperature resistance with a very fast momentum relaxation time scale τ . In contrast, we claim that linear in temperature resistance is caused by quantum interference (Cooperon) loops with very large areas, and that increasing temperature controls the resistance by progressively

cutting off these loops via decoherence. In particular, linear magnetoresistance has been observed in bad metals at temperatures of 1000 K, and we understand this as clear evidence that quantum interference and quantum coherence continue up to the same temperatures, albeit with a number of harmonics that decreases steadily as temperature increases.

We have made one assumption throughout this discussion: that the phase factor associated with flux through electron and hole loops is responsible for linear resistance, and not the Zeeman coupling between field and spin, which we have neglected. As we have discussed earlier, disordered transport is mediated by the single particle density matrix $\rho(x)$. The main effect of spin on disordered transport is that $\rho(x)$ contains both a spin singlet (charge) and a spin triplet (spin polarization). The charge singlet contribution to WL/WAL decreases the resistance, while the spin triplet contribution to WL/WAL increases the resistance.^{22,31} If the charge singlet or spin triplet relaxation time τ_s and τ_t are short then these contributions are reduced. In particular, when the charge singlet relaxes more slowly than the spin triplet, i.e. when $\tau_s \gg \tau_t$, then the charge singlet contribution dominates and the net effect is a decrease in resistance, i.e. weak antilocalization (WAL). This combination of lifetimes $\tau_s \gg \tau_t$ is found when spin rotation symmetry is broken more strongly than than time reversal symmetry, as is the case with strong spin-orbit coupling. On the other hand, when time reversal symmetry is not more favored than spin rotation, and the charge singlet and spin triplet relaxation time scales $\tau_s \sim \tau_t$ are similar, then the spin triplet dominates and the net effect is the opposite, weak localization (WL). In summary, WAL occurs when the spin triplet relaxes quickly so that conduction is mediated by charges which effectively have zero spin, while WL occurs when both the charge singlet and spin triplet contribute to conduction.

Magnetic field is a perfect diagnostic tool for distinguishing between WAL and WL: WAL results in the resistance increasing with field, while WL results in the resistance decreasing with field. Experimental observations of linear magnetoresistance universally find that resistance increases rather than decreases with field, as seen in WAL. We therefore conclude that in linear resistance materials the spin triplet relaxation time τ_t is short while the charge singlet lifetime τ_s is significantly longer, that only the charge singlet and not the spin triplet contributes to conduction, and therefore that the Zeeman effect is not relevant to conduction.

Section I will start from charge conservation and show that it allows one to start with experimental measurements of magnetic field dependence and then obtain rigorous information about the areas of electron and hole loops. Next section II applies this methodology to compare the areas of loops in Landau levels, SdH oscillations, WL/WAL, linear magnetoresistance, and Levy flights. Section III shows how quantum coherence causes resistance to be linear in field and temperature and discusses

coefficients that can be measured experimentally, and section IV wraps up with a few final thoughts.

I. GEOMETRIC ANALYSIS OF ELECTRON AND HOLE LOOPS

Charge conservation is a fundamental feature of nature which has been subjected to intense scrutiny and has been found to be obeyed to extreme precision. Two strategies are available to engineer a theory to correspond to this experimental reality. One strategy is to select a set of quantum mechanical states available to the system, and a Hamiltonian which describes the system's ground state and dynamics. In the process of building the states and the Hamiltonian, one enforces a constraint: all states must have the same total charge, and the Hamiltonian may not change that charge. This approach is very powerful, and has shown extreme versatility in building models of the essential physics of many systems. These include simplified models where the electron's position is restricted to an integer number of discrete values and therefore electron paths are series of discrete jumps. However this approach has the weakness that charge conservation is essentially imposed by fiat, and that its fundamental connection to the geometry of electron and hole loops is lost.

To capture the geometry of electrons moving in the real world, it is necessary to start from the symmetries of the real world. These include continuous translation, i.e. the electrons' ability to move smoothly along continuous paths instead of jumping from position to position, and Poincare symmetry, the ability to smoothly change direction in the four dimensional manifold of space and time. The class of theories which unite these symmetries to quantum mechanics, relativistic quantum field theory, is our starting point for understanding the connection between charge conservation and geometry.

An early and essential result of relativistic quantum field theory was the Dirac equation, which predicted the existence of holes. Soon afterwards quantum electrodynamics was formulated, in which the principle of gauge invariance is key to guaranteeing charge conservation. Later the constraints of internal consistency (renormalizability, unitarity, etc.) and of experimental data resulted in the standard model, in which gauge invariance is elevated to a guiding principal that is key to all electronic interactions. The standard model incorporates quantum electrodynamics, and preserves its treatment of charge conservation of electrons and holes, which is based on gauge invariance.

Gauge invariant theories are built in two steps. The first step is adding a gauge field: a $U(1)$ phase $\phi(\vec{x})$ which depends on position. This phase modifies the momentum operator which describes translational motion, so that as an electron moves along its path, its phase is multiplied by the difference between the phases $\exp(i\phi)$ at the electron's final position and its initial position. The second

and final step toward building a gauge invariant theory is the requirement that the theory be invariant under arbitrary changes of the gauge field. This is essentially a mathematical shorthand for imposing a restriction on the structure of every physical observable. The only way to build an observable \mathcal{O} which is independent of $\phi(\vec{x})$ is by requiring each electron contributing to the observable to return to its starting position, forming closed loops. Because the final and initial positions are the same, the difference in phase $\exp(i\phi)$ between start and end is exactly zero, and therefore observables built from closed loops do not depend on $\exp(i\phi)$; they are gauge invariant. The actual shape and size of the loops, and also the number of loops, is completely unrestricted by gauge invariance; the emphasis is on their closed nature.

In relativistic quantum field theory the electron paths move through space-time, and the requirement to return to the origin does not mean only that an electron must reverse its motion in space. Each electron is also required to reverse its direction in time, so it can eventually return to its starting time. From one point of view this reversal of direction is simply a manner of pulling a loop's path back to its origin, but from another point of view the reversal of time-direction is the meeting (creation or annihilation) of a particle-hole pair. In other words, one can adopt a vocabulary that avoids discussing electrons moving backwards-in-time, but only at the cost of saying that for every electron [moving in forward in time] there is also a hole. The hole is thought of as moving forward in time, but it has exactly the same mathematical and physical consequences as an electron moving backward in time. The net effect is that instead of talking about electrons tracing loops in space-time, one requires that electrons and holes are always produced and destroyed in pairs. If one takes the hole and electron paths together one finds that they always add up to loops in space-time. This loop structure is an immediate and unavoidable consequence of combining gauge invariance with special relativity.

Gauge invariance ensures charge conservation in a way that is so powerful that it seems almost trivial, as follows. First it requires that that observables be made out of space-time loops. Secondly we divide up each space-time loop into segments that move forward in time [electrons], and segments that move backward in time [holes]. Thirdly we assign charge $-e$ to electrons and charge $+e$ to holes. Fourthly we note that the loop structure implies that electrons are always created or destroyed with corresponding holes, in pairs. We thus arrive at charge conservation: this structure of pair-wise creation/destruction manifestly conserves total charge.

A. Coupling Magnetic and Electric Fields to Loops

In relativistic quantum field theory the effect of magnetic and electric fields on electrons is mediated by the minimal coupling: the momentum operator p^μ is replaced by $p^\mu - eR^\mu$, where the gauge potential $R^\mu = \partial^\mu\phi$ is the

first derivative of the gauge phase $\phi(\vec{x})$. The electric and magnetic fields \vec{E}, \vec{B} are encoded in $R^\mu = (\phi/c, \vec{R})$ via $\vec{E} = -\vec{\nabla}\phi - \partial\vec{R}/\partial t$ and $\vec{B} = \vec{\nabla} \times \vec{R}$. This minimal coupling is required to construct a gauge invariant continuum theory - it is necessary to ensure that when an electron moves from a starting position to a final position, it is multiplied by the difference in phases $\exp(i\phi)$ at the two positions.

The minimal coupling implies that as an electron or hole traces its path, the only effect of electric and magnetic fields is to introduce a multiplicative factor, the Wilson loop $W_\gamma = \exp(i \oint_\gamma ds_\mu R^\mu)$.^{32,33} The line integral $\oint_\gamma ds_\mu$ is taken along the electron/hole path, denoted by γ . It is a loop integral because electron and hole paths are required to form loops.

When several electron-hole loops occur the line integrals of each loop add up, and the multiplicative factors $\exp(i \oint_\gamma ds_\mu R^\mu)$ multiply each other. Therefore we shift the notation from γ which specifies a single loop to Γ , which specifies the paths traced by a set of one or more electron and hole loops. The total effect of all the loops together is to multiply by $W_\Gamma = \exp(i \oint_\Gamma ds_\mu R^\mu)$, where the line integral $\oint_\Gamma ds_\mu$ is the sum of each of the loop integrals in Γ . Gauge invariant observables are built from sums in which each term of the sum has a particular set of electron-hole loops Γ and is weighted by the corresponding Wilson loop W_Γ .

By Stokes' theorem the phase $\oint_\Gamma ds_\mu R^\mu \equiv \Phi_\Gamma$ in the Wilson loop is equal to the electro-magnetic flux through the one or more loops specified by Γ . In other words, the line integral $\oint_\Gamma ds$ over loops Γ is equivalent to a flux integral $\int_\epsilon dS$ over the surfaces ϵ bounded by the loops. Mathematically $\oint_\Gamma ds_\mu R^\mu = \Phi_\Gamma = \int_\epsilon dS_{\mu\nu} F^{\mu\nu}$. Here $F^{\mu\nu} = \partial^\mu R^\nu - \partial^\nu R^\mu$ is the electromagnetic field tensor whose components are equal to the electric and magnetic fields, and $dS_{\mu\nu}$ is the infinitesimal surface tensor for a surface embedded in four-dimensional space-time. When the surfaces ϵ are all fixed to a particular time t this flux simplifies to the magnetic flux $\Phi_\Gamma = \int_\epsilon d\vec{S} \cdot \vec{B}$, where now $d\vec{S}$ is the surface infinitesimal in three-dimensional space and \vec{B} is the magnetic field.

In atomic units where $e = \hbar = 1$ the phase Φ_Γ controlling the Wilson loop $W_\Gamma = \exp(i\Phi_\Gamma)$ is equal to the electromagnetic flux. Because both the phase and the flux are strictly the argument of an exponential, they must be unit-free. In turn the units of electromagnetic field $F^{\mu\nu}$ must be the inverse of the units of the area infinitesimal $dS_{\mu\nu}$. This is the fundamental reason why the electromagnetic field tensor $F^{\mu\nu}$, and magnetic field \vec{B} in particular, have units of inverse area.

We formalize these ideas using the loop representation of observables.³⁴ The previous discussion can be summarized by the statement that every physical observable $\mathcal{O}_i(\vec{B})$ must be written as

$$\mathcal{O}_i(\vec{B}) = \sum_\Gamma \langle \mathcal{O}_i | \Gamma \rangle \exp(i\Phi_\Gamma) \quad (1)$$

where \sum_{Γ} is a sum over all the Wilson loops which contribute to the observable \mathcal{O}_i , and $\langle \mathcal{O}_i | \Gamma \rangle$ is the weight with which a particular Wilson loop Γ contributes to \mathcal{O}_i . This weight is determined by both the observable and by the kinetics and interactions of the electrons tracing the loops in Γ .

B. The non-relativistic limit

In relativistic quantum field theory the electron-hole pair follows a path which curves through space time and finally returns to its origin. The energy of the electron and the energy of the hole, taken separately, vary throughout their motion around the loop.

The non-relativistic limit is taken by assuming that the energies of the electron and hole are almost constant and remain very near their rest energy/mass. Obviously this requires a strict conceptual division between electron and hole. In this limit the Dirac equation, describing both electron and hole, simplifies to the Pauli equation which describes either the electron or the hole.

Because of the non-relativistic limit's special treatment of the time dimension, electric field drops out of the minimal coupling and takes a separate role in the Pauli equation, and is joined by the $e\vec{\sigma} \cdot \vec{B}$ Zeeman term. The remaining minimal coupling is $\vec{p} - e\vec{R}$, where \vec{R} is the gauge field determining the magnetic field by $\vec{B} = \vec{\nabla} \times \vec{R}$. The minimal coupling coupling produces Wilson loops $\exp(i\Phi_{\Gamma})$ where the flux $\Phi_{\Gamma} = \int_{\epsilon} d\vec{S} \cdot \vec{B}$ depends only on magnetic field not electric field.

In the non-relativistic limit magnetic field affects electronic motion not only through Wilson loops but also via the Zeeman term. As we have argued earlier, in the linear resistance systems which are our interest the spin triplet relaxation time is τ_t is short compared to the spin singlet relaxation time τ_s . Therefore in linear resistance systems spin and the Zeeman term do not contribute to electronic transport over long distances, and observables measuring transport depend on magnetic field only via Wilson loops, not via the Zeeman term.

C. External Fields and the Loop Area Distribution

We specialize to the case of a uniform magnetic field \vec{H} originating externally to the sample, which we will call $\vec{B}^{ext} \equiv \vec{H}$. We consider the effect of \vec{B}^{ext} on the one or more electron-hole loops specified by Γ . Each electron-hole loop experiences not only the external field \vec{B}^{ext} , but also magnetic field generated by the electron-hole loops within the sample. The total field, including both external field and the field generated by the sample, is called \vec{B} . Total field \vec{B} is related to external field \vec{B}^{ext} via $\vec{B} = \mu_0 \vec{B}^{ext} + \mu_0 \vec{M}$, where \vec{M} is the magnetization. μ_0 is the vacuum permeability, which we will drop for simplicity. In diamagnetic materials, including

superconductors, \vec{B} is smaller than \vec{B}^{ext} , while in paramagnetic materials \vec{B} is larger than \vec{B}^{ext} . We separate the magnetic flux through a Wilson loop into a contribution Φ_{Γ}^{int} from loops within the sample and a contribution $\Phi_{\Gamma}^{ext} = \int_{\epsilon} d\vec{S} \cdot \vec{B}^{ext}$ from external field. Therefore in an external magnetic field observables can be written as

$$\mathcal{O}_i(\vec{B}^{ext}) = \sum_{\Gamma} \langle \mathcal{O}_i | \Gamma \rangle \exp(i\Phi_{\Gamma}^{ext}) \quad (2)$$

The phase Φ_{Γ}^{int} from electron-hole loops within the sample is now packaged inside the weight $\langle \mathcal{O}_i | \Gamma \rangle$.

Because the external field \vec{B}^{ext} has uniform direction and magnitude, it is useful to assign to each Wilson loop a vector-valued cross-section $\vec{A}_{\Gamma} = \int_{\epsilon} d\vec{S}$, which is a vector generalization of the Wilson loop's surface area. This area vector depends only on paths traced by the loop Γ , not on the shape of the the surfaces ϵ which are bordered by Γ . The magnetic flux through Γ then simplifies to the dot product of the area \vec{A} with the external field \vec{B}^{ext} ; $\Phi_{\Gamma} = \vec{A}_{\Gamma} \cdot \vec{B}^{ext}$. This leads to our central result:

$$\begin{aligned} \mathcal{O}_i(\vec{B}^{ext}) &= \int d\vec{A} \mathcal{O}_i(\vec{A}) \exp(i\vec{A} \cdot \vec{B}^{ext}), \\ \mathcal{O}_i(\vec{A}) &\equiv \sum_{\Gamma} \langle \mathcal{O}_i | \Gamma \rangle \delta(\vec{A}_{\Gamma} - \vec{A}) \end{aligned} \quad (3)$$

In other words, every physical observable can be resolved into contributions corresponding to specific areas \vec{A} , each with weight $\mathcal{O}_i(\vec{A})$:

$$\mathcal{O}_i(\vec{A}) = \int \frac{d\vec{B}^{ext}}{(2\pi)^3} \mathcal{O}_i(\vec{B}^{ext}) \exp(-i\vec{A} \cdot \vec{B}^{ext}) \quad (4)$$

In summary, equations 3 and 4 state that measurements of an observable $\mathcal{O}_i(\vec{B}^{ext})$'s magnetic field dependence give direct and rigorous information about the areas traced out by electron loops within a sample, simply by performing a Fourier transform. The resulting loop area distribution $\mathcal{O}_i(\vec{A})$ completely describes how different loops contribute. In particular, the external field \vec{B}^{ext} is conjugate to a specific area \vec{A} , $A_i = (\vec{B}_i^{ext})^{-1}$, and there is no possibility that any process could renormalize this relation.

From a theorist's point of view, the problem of how to perform a regularized sum over loops \sum_{Γ} , i.e. how to control both long distance and short distance contributions to the sum, remains in general unsolved. This makes evaluation of the sum over loops \sum_{Γ} in equations 1 and 3 a difficult task. It is therefore both remarkable and encouraging that we can measure the sum experimentally and directly using equation 4; experimental measurements of the loop area distribution $\mathcal{O}_i(\vec{A})$ can lead the way in guiding theorists to correct procedures for performing the sum over loops.

II. COMPARISON OF LOOP AREA DISTRIBUTIONS

Throughout the remainder of this paper $\vec{B} = \vec{B}^{ext} = \mu_0 \vec{H}$ means the external magnetic field, and $B = |\vec{B}|$ is its magnitude.

A. Landau levels and SdH Oscillations

To illustrate the transformation from experimental observables to loop area distributions, consider the case where the dominant energy scale is the Fermi level E_F , in which case a delta function - the first Landau level - will be found in $G_{xx}(B)$ at $B^{-1} = \frac{1}{2}A_F$. Here $2\pi/A_F \propto 2\pi E_F$ is the cross-section of the Fermi surface.³⁵ The loop area distribution is therefore a cosine $G_{xx}(A) \propto \cos(A/\frac{1}{2}A_F)$, which means that loops with every area contribute to the conductance and that there is ringing corresponding to the characteristic Fermi area A_F .⁷⁷

The most interesting aspect of this result is that quantum coherence causes the first Landau level to be repeated exactly at characteristic areas $(N + 1/2)A_F$, with the N -th level's height proportional to N . The repetitions are manifested as a hierarchy of additional Landau level delta functions in $G_{xx}(B)$, as illustrated in Figure 1a. Figure 1b shows the loop area distributions $G_{xx}(A)$ of the Landau levels. The N -th Landau level is a cosine $\cos(A/(N + \frac{1}{2})A_F)$ with period equal to $(N + 1/2) 2\pi$ times the characteristic area A_F . In mathematical terminology, the N -th Landau level is simply the N -th harmonic of the lowest Landau level. Speaking more plainly, quantum coherence ensures that if an electron can complete a loop once, then it can repeat that same loop any number of times.

The only limit to these repetitions (harmonics) is decoherence caused by the scattering energy scale Γ or temperature T , which causes a decay in the loop area distribution.³⁶ Decoherence broadens the Landau levels into peaks with width Γ, T , which eventually merge into SdH oscillations. These oscillations have equal height instead of the height proportional to N seen in Landau levels. They decay exponentially when the value of $B = N^{-1}A_F^{-1}$ descends to Γ, T , and their loop area distribution also decays exponentially at areas larger than Γ^{-1}, T^{-1} .^{36,78}

B. Weak Antilocalization

We now investigate 2-D WL/WAL, whose magnetoconductance $G_{xx}^{WL}(B)$ has been studied extensively. We will show that the WL/WAL loop area distribution varies inversely with area i.e. it obeys $G_{xx}^{WL}(A) \propto A^{-1}$. At magnetic fields less than the inverse cutoff $q_C B < 1/L_{max}^2$ the conductance $G_{xx}^{WL}(B)$ is controlled by the cutoff: it quickly transitions to zero, and this transition

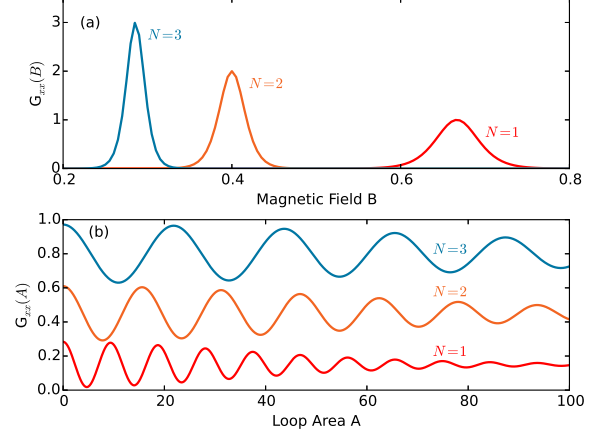


FIG. 1: (Color online.) Quantum coherence and the hierarchy of Landau levels. Panel (a) shows the magnetoconductance $G_{xx}(B)$ of the $N = 1, 2, 3$ Landau levels and panel (b) shows their loop area distributions $G_{xx}(A)$, which have been vertically shifted for clarity.³⁶ Quantum coherence is responsible for producing higher harmonics of the lowest Landau level, causing higher Landau levels at multiples $(N + \frac{1}{2})A_F$ of the characteristic area $A_F = E_F^{-1}$. Decoherence, i.e. loss of quantum coherence, is caused by either the scattering energy scale Γ or the temperature T . Decoherence widens peaks in $G_{xx}(B)$, suppresses $G_{xx}(A)$ at large A , and completely suppresses oscillations when the field B is as small as Γ, T . $E_F = 1$, $\Gamma = 0$, $T = 0.05$.

is quadratic in B because time reversal symmetry requires that G_{xx} be even under $B \rightarrow -B$. At larger fields $q_C B > 1/L_{max}^2$ the magnetoconductance of a 2-D spin singlet is a logarithm $G_{xx}^{WL}(B) \propto -\ln B$. This logarithmic form, which will be our focus here, is robust and ubiquitous. If spin or orbital degrees of freedom are in play then the logarithmic conductance seen in the singlet generalizes simply to a sum of logarithms corresponding to different components of the density matrix including the spin singlet, triplet, etc. The logarithmic conductance is seen for both Dirac and $p^2/2m$ dispersions, for both lattice and continuum models, for both short and long range scattering, and for a wide variety of quasi-2-D geometries.^{22,37-49} The logarithm is found in all 2-D systems that are in the diffusive regime, i.e. all 2-D systems whose size is larger than the momentum relaxation length caused by scattering.

The reason that the same form of $G_{xx}^{WL}(B)$ is universally found in diffusive 2-D systems is that at distances exceeding the momentum relaxation length the Cooperon loses all information about momentum and kinetics, and therefore its trajectory is simply a 2-D random walk. When spin or orbital degrees of freedom are in play the Cooperon carries several species of random walkers (e.g. a spin singlet and a spin triplet), but each of the species is still performing a simple random walk. The WL/WAL magnetoconductance signal is determined by Cooperon

trajectories which return to their origin, forming loops. Quantum coherent repeats of loops do not contribute because the Cooperon's momentum is random and therefore even when a Cooperon returns to its origin it does not have the same momentum that it started with. Since the trajectories of these Cooperon loops are simply random walks, the magnetoconductance signal has the same form in all 2-D diffusive systems.

The fact that the universal form of the magnetoconductance $G_{xx}^{WAL}(B) \propto \ln B$ is logarithmic was first determined by Ref.²². Ref.²² starts with a description of how scattering changes the motion of the electronic wavefunction $|\psi\rangle$ and its complex conjugate $\langle\psi|$, and then uses this information to derive the behavior of the Cooperon, which is a pairing of $|\psi\rangle$ with $\langle\psi|$. It is found that the spin singlet component of the Cooperon is simply a random walker and that every random walk returning to the origin contributes with equal weight to the WAL conductance $G_{xx}^{WAL}(B)$. Mathematically this is expressed by writing the Cooperon Green's function as the inverse of a Laplacian operator which expresses how individual steps in the walk are taken. The WAL conductance is proportional to the probability that the Cooperon will return to its origin; mathematically it is the diagonal $\vec{x} = \hat{x}$ matrix element of the Cooperon Green's function. At zero field $G_{xx}^{WAL}(B = 0)$ is simply the probability that random walkers will return to their origin, while non-zero field causes each each walker trajectory to be reweighted by a Wilson loop phase factor. Calculation of the Cooperon spin triplet component is almost identical to that of the singlet - the main difference is that the triplet contribution to G_{xx} is multiplied by -1 , producing weak localization instead of weak antilocalization.

We emphasize the fact that all trajectories contributing to the Cooperon's spin singlet component contribute with the same weight, with no phase factor from kinetics, scattering, potentials, or time evolution. Likewise, all trajectories contributing to the Cooperon's triplet component contribute with the same weight. In other words, although the Cooperon describes a special kind of quantum interference process that is exhibited by electrons, the actual behavior of a Cooperon is no different than that of a purely classical random walker. No phase information enters in because a Cooperon is a pairing of $|\psi\rangle$ with $\langle\psi|$, and their phases cancel each other. Therefore the Cooperon evolves as a classical random walker, and calculations of $G_{xx}^{WAL}(B)$ look purely classical. All Cooperon trajectories (of the singlet, or of the triplet) contribute with the same sign and weight. One very important consequence is that the loop area distribution $G_{xx}^{WAL}(A)$ of the Cooperon singlet (or triplet) trajectories has only one sign, like a purely classical probability distribution. Calculation of WL/WAL is isomorphic to calculating return probabilities of a purely classical walker.

This picture of a purely classical Cooperon is modified in samples with sizes approaching the localization length, where the conductance is reduced to the order of the

universal conductance quantum G_0 . At this long length scale processes coupling two or more Cooperons become important. However the systems which show the *weak* localization and antilocalization which is our focus here lie far from the localized limit, so that the WL/WAL contribution remains at the level of simple random walks without multi-Cooperon processes.

We demonstrate here that the Fourier transform of the logarithmic WL/WAL conductance $G_{xx}(B) \propto \ln B$ varies inversely with area, i.e. that the loop area distribution obeys $G_{xx}(A) \propto A^{-1}$. In other words the Fourier transform of $-\ln B$ is A^{-1} and, vice versa, the inverse Fourier transform of A^{-1} is $-\ln B$. The main difficulty is controlling the ultraviolet and infrared cutoffs, so we perform the demonstration three ways. First, we use purely dimensional analysis: $G_{xx}(A) = (2\pi)^{-1} \int dB \exp(-iAB) \ln B$. Therefore $G_{xx}(A)$ must carry units of inverse area; it must be equal to A^{-1} times some function that depends only on dimensionless quantities.

Second, we use specific functional forms for $G_{xx}(A)$ and carry out analytically the inverse Fourier transform from $G_{xx}(A)$ to $G_{xx}(B)$. For instance, we consider hard cutoffs at A_0 and A_{max} , with $G_{xx}^{WAL}(A) = A^{-1}$ for $A_0 < A < A_{max}$. With these cutoffs we arrive at $G_{xx}^{WAL}(B) \approx R_0 - \ln|q_C B| + (q_C B A_0)^2/4$ for $1/A_{max} < q_C B < 1/A_0$, where $R_0 = -\gamma_E - \ln|A_0|$ and γ_E is the Euler-Mascheroni constant. Here R_0 should be adjusted to zero, as a regularization compensating for the hard cutoffs, to replicate the well-known fact that the WAL (Cooperon spin singlet) contribution to the conductance is always positive for all values of B , and that the triplet WL contribution is always negative. The appendix imposes several other cutoffs on $G_{xx}^{WAL}(A) = A^{-1}$, in each case performs the Fourier transform exactly, and in each case obtains logarithmic forms for $G_{xx}^{WAL}(B) = \int dA \exp(iAB) A^{-1} \propto -\ln B$.

Lastly, since Ref.²² and many subsequent works have established that the magnetoconductance $G_{xx}^{WAL}(B)$ of a 2-D random walking Cooperon is logarithmic, a demonstration that the loop area distribution of 2-D random walkers is $G_{xx}^{WAL}(A) \propto A^{-1}$ is sufficient to show that the Fourier transform of $-\ln B$ is A^{-1} . Figure 2a summarizes the results of extensive numerical Monte Carlo simulations of random walks, all of which verify that the loop area distribution of random walks which return to their origin scales with A^{-1} . We use an infinite 2-D square lattice, and define the lattice spacing equal to one. The walkers take steps which are chosen from a Gaussian distribution with mean step length $l = 4\sqrt{2}, 8\sqrt{2}$, and an upper bound (IR cutoff) to the loop areas is supplied by limiting the walk length to 5×10^5 . We count the walkers which return to their origin, compute the area of the loop traversed by each walker, and histogram the area distribution $G_{xx}(A)$. Panel (a) shows $G_{xx}(A)$, multiplied by A . The plateaus of constant $G_{xx}(A) \times A$ extending over several orders of magnitude verify that 2-D random walks follow an A^{-1} loop area distribution. We

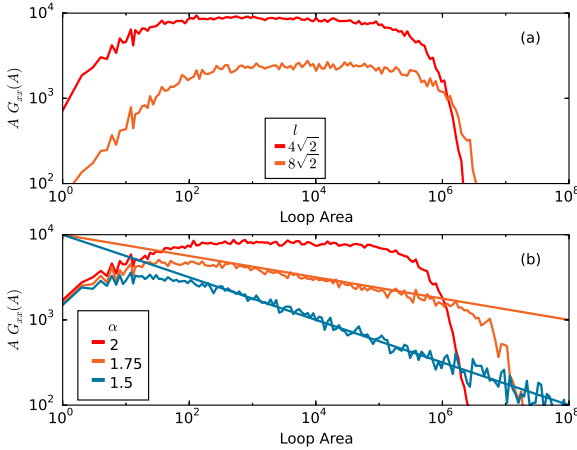


FIG. 2: (Color online.) The Cooperon's loop area distribution $G_{xx}(A)$ obtained by Monte Carlo simulations. Panel (a) shows $G_{xx}(A)$, multiplied by A , of standard 2-D random walks with Gaussian-distributed steps having average length $l = 4\sqrt{2}, 8\sqrt{2}$. The plateaus extending over several orders of magnitude verify that 2-D random walks follow an A^{-1} loop area distribution. The IR cutoff is caused by limiting the walk length to 5×10^5 . Panel (b) shows that Levy flights have a loop area distribution which decays faster than A^{-1} . α is the stability parameter of the Levy alpha-stable distribution which controls the step lengths. $\alpha = 2$ produces Gaussian-distributed steps, and when α is decreased below 2 the distribution develops a heavy tail of very long steps. The straight lines are for $10^4 \times A^{-0.125}$ and $10^4 \times A^{-0.25}$, and their agreement with the Monte Carlo data shows that $G_{xx}(A) \propto A^{-2+\alpha/2}$. $l = 4\sqrt{2}$ and the IR cutoff is 5×10^5 , 1.5×10^6 , and 5×10^6 for the $\alpha = 2, 1.75, 1.5$ results.

have verified that similar results are found with other cutoffs and other probability distributions governing the step lengths, and a similar numerical Monte Carlo simulation of 2-D random walks has also verified the A^{-1} loop area distribution.⁵⁰ These numerical demonstrations of the A^{-1} loop area law again verify that the Fourier transform of $-\ln B$ is $G_{xx}(A) \propto A^{-1}$, and vice versa.

C. Linear magnetoresistance

This result can be reversed and applied to the case of linear magnetoresistance, where $G_{xx}(B) \propto B^{-1}$. We established above that the inverse Fourier transform of A^{-1} is $-\ln B$; interchanging A with B shows that the loop area distribution corresponding to linear magnetoresistance is logarithmic, $G_{xx}(A) \propto -\ln A$. This profile, whose broad features are general for any roughly linear resistance, is remarkably different from the A^{-1} distribution that governs loops generated by random walks. It has fewer small loops and many more large loops; a small head and a very long tail. We emphasize that the logarithmic loop area distribution is a rigorous result and can be inferred whenever a linear magnetoresistance is

seen, no matter what physical mechanism is responsible for producing the loops.

Both the logarithmic area distribution $-\ln A$ associated with linear magnetoresistance and the standard WAL result $1/A$ are monotonically decreasing functions of A , without any hint of oscillations. In striking contrast the area profiles of Landau levels and SdH oscillations show many repeated changes in sign as the loop area A is varied. This is very compelling evidence that linear magnetoresistance is caused by Cooperons, i.e. paired particles and holes scattering together, rather than by any species of single-particle motion. The phase of single electrons and holes oscillates very rapidly at the Fermi wavelength, which is the ultimate reason why the loop area distribution of Landau levels exhibits an oscillating sign. In contrast the Cooperon is a quasi-classical object that does not show phase fluctuations at length scales up to the localization length, which is far in excess of the Fermi wavelength. The Cooperon's singlet and triplet components therefore have very smooth single-sign loop area distributions, unlike the loop area distributions of Landau levels and SdH oscillations. The fact that the linear magnetoresistance's $-\ln A$ loop area distribution is smooth and single-signed clearly identifies linear magnetoresistance as being caused by Cooperons, not by single-particle motion.

If, as we have suggested, WAL caused by interaction-induced scattering is responsible for the bad metals' linear resistance, then translational symmetry is broken in these materials. Specifically, the electronic and hole carriers fluctuate and break translational symmetry. Later in this text we estimate that in order to allow Cooperons to complete their loops, the fluctuations must persist on the scale of picoseconds or longer. As a consequence a diffuse (non-momentum-conserving) component should be seen in the single particle density of states and in excitation spectra such as ARPES, when analyzed as functions of momentum.

D. Levy Flights and 3-D

The $1/A$ decay seen in 2-D random walks seems to be the slowest decay that can be produced by purely stochastic random walks. Figure 2b shows that if instead diffusion is replaced by Levy flights where step lengths follow a distribution including both short and very long steps, the result is again a steeper decay than A^{-1} , because long steps tend to decrease the probability that the walker's path will complete a loop. Here we again use a 2-D square lattice, choose random steps from a probability distribution, and impose an IR cutoff l on the maximum path length. The only difference from Figure 2a is that instead of choosing steps from a Gaussian probability distribution to produce a random walk, we choose steps from the Levy alpha-stable distribution, producing Levy flights where most steps are short but some steps are very long. The Levy alpha-stable distribution is controlled by

the Levy distribution stability parameter α which we give values $\alpha = 2, 1.75, 1.5$. When $\alpha = 2$ it reduces to the Gaussian distribution, and when α is decreased below 2 the distribution develops a heavy tail of very long steps. Panel 2b plots $G_{xx}(A) \times A$. At $\alpha = 2$ we see again the plateau signaling the $1/A$ area decay law of random walks. At $\alpha = 1.75, 1.5$ the loop area distribution decays faster than A^{-1} , tilting the plateau. We superimpose straight lines for $10^4 \times A^{-0.125}$ and $10^4 \times A^{-0.25}$, and their agreement with the $\alpha = 1.75, 1.5$ Monte Carlo data shows that $G_{xx}(A) \propto A^{-2+\alpha/2}$. In summary, Levy flights steepen the area law decay, taking it further from the very slow $\ln A$ decay necessary to produce linear magnetoresistance. Moreover, increasing the dimensionality above two dimensions produces a steeper decay, $A^{-3/2}$ in 3-D.⁵¹ Therefore neither changing the step distribution nor changing the dimensionality can reproduce the $\ln A$ tail seen in linear magnetoresistance systems.

We note that in very strong magnetic fields where the magnetic length $l_H = \sqrt{\hbar c/eB}$ is smaller than the mean free path a a \sqrt{A} area law is obtained at areas smaller than l_H^2 .⁵²⁻⁵⁵ However this produces a $1/\sqrt{B}$ magnetoresistance, not a linear signal, and is strictly a large-field behavior, unlike experiments where linear magnetoresistance starts at small fields.

III. WEAK ANTILOCALIZATION WITH QUANTUM COHERENCE

Since linear magnetoresistance can not be explained by random walks or by Levy flights, we propose instead that the Cooperons responsible for linear magnetoresistance do follow random walks, but with the special feature that they maintain quantum coherence, allowing them to repeat their loops many times, in the same way that Landau levels are repeated in a hierarchy at $(N + \frac{1}{2})A_F$. This depletes the loop distribution's head, because if a loop area distribution has a UV cutoff at A_0 , then its $N = 2$ first repetition will have a higher UV cutoff at $2A_0$, its second repetition will have its cutoff at $3A_0$, etc. Therefore between A_0 and $2A_0$ the total loop area distribution will have a contribution from only the base $N = 1$ loop distribution, while at larger areas higher and higher N will contribute. For example, consider the case of 2-D random walks with hard cutoffs at A_0 and A_{max} and $G_{xx}^1(B, A_0, A_{max}) = \int_{A_0}^{A_{max}} dA \cos(q_C B A)/A$. Allowing up to N repetitions with inverse weighting and regularizing with γ_E obtains $G_{xx}(B) = \gamma_E + \sum_{n=1}^N n^{-1} G_{xx}^1(B, nA_0, A_{max})$. Figure 3a compares this loop area distribution to the diffusive $1/A$ profile produced by random walks without coherence, showing that it has the required small head and long tail. Figure 3b shows the resulting linear magnetoresistance, which is proportional to $R_{xx}(B) - R_{xx}(B = 0) \approx \pi q_C B A_0$ for $1/A_{max} < q_C B < 0.2/A_0$.

In this example, a proof of principle about how to obtain linear magnetoresistance, we chose an abrupt IR cut-

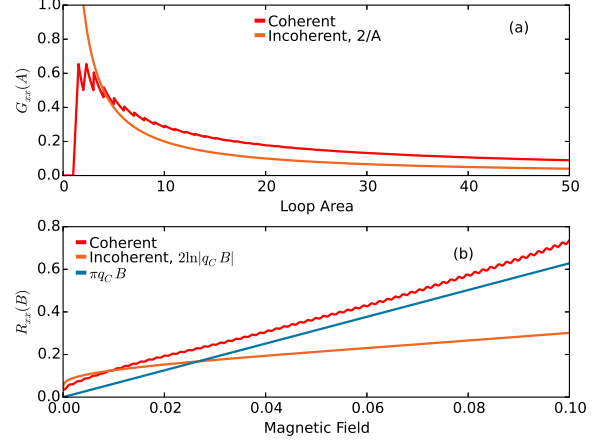


FIG. 3: (Color online.) Linear magnetoresistance from quantum coherence. The red lines show the results when quantum coherence allows loops to repeat up to $N = 100$ times. They can be compared to the orange lines which show standard behavior without quantum coherence. Panel (a) shows the loop area distribution $G_{xx}(A)$, where the quantum coherent distribution (red line) clearly has a small head and long tail as compared to the standard distribution (orange line). Panel (b) shows the resistance $R_{xx}(B)$. The quantum coherent result (red line) compares nicely to the blue straight line with slope πq_C . $A_0 = 1$, and the sharpness of the hard IR cutoff at $A_{max} = 2000$ causes the ripple in the quantum coherent result. The orange line gives a standard logarithmic curve, $R_{xx}(B) = (0.1 - 2 \ln |q_C B|)^{-1}$.

off at A_{max} and an abrupt UV cutoff at A_0 . The true forms of these cutoffs will be material dependent. In Fig. 3b superimposed on the linear signal one sees a small amplitude fast ripple, which is ringing caused by the abrupt IR cutoff. This ripple has been seen in Ref.¹, signaling that a sharp IR cutoff was present in that experiment. However in most experimental data on linear resistance a ripple is not visible, indicating either a smooth IR cutoff or that magnetic field was not sampled at fine enough resolution. At large fields the form of the UV cutoff also manifests in the signal's behavior. Our sharp UV cutoff causes strong ringing at large fields $q_C B > 0.2/A_0$ [not shown in Fig. 3b] which overwhelms the linear magnetoresistance signal, but with a suitably chosen UV cutoff the linear growth will extend to larger B .

We emphasize that a power law area distribution can always be given a depleted head and long tail by invoking quantum coherence and allowing loop repetitions. The form of the UV and IR cutoffs, the relative weight of each repetition, and even the base loop area distribution $G_{xx}^1(A)$ may be specific to the scattering source and to the mechanism responsible for Cooperon coherence. Nonetheless there are only two fundamental requirements: a scattering process producing an area distribution with broad support across a range of areas, and quantum coherence allowing Cooperon loops to repeat in

a hierarchy like that of Landau levels.

A. Mechanisms for Preserving Quantum Coherence

Ordinarily 2-D Cooperons do not display loop repetitions retracing their path two or more times, unlike the loop repetitions which are seen in Landau levels and SdH oscillations. The fundamental reason is that when a Cooperon returns to its starting point it does so with a momentum that is different from its original momentum. Therefore on the second time around the Cooperon leaves the origin moving in a direction that is different from its first time around.

There are two notable exceptions which prove that under the right circumstances Cooperons are able to maintain quantum coherence and show quantum loop repetitions similar to the higher harmonics seen in Landau levels and SdH oscillations. The most notable exception is 1-D systems with static disorder. In 1-D the Cooperon's particle and hole are constrained to follow the same path, and the static disorder means that their energies never change, and neither does the magnitude of their momenta. Therefore when a Cooperon returns to its starting point it can easily repeat the same exact loop that it has just ended, starting with a momentum that has the same magnitude and direction as before. As a result Cooperon-mediated quantum interference dominates the behavior of 1-D and quasi 1-D systems: once the system's length L increases enough so that the usual classical $1/L$ Ohm's law decay brings the conductance down to one conductance quantum G_0 , quantum interference takes over. This can take two forms. In most systems the conductance decay transitions from the $1/L$ Ohm's law to the exponential decay characteristic of Anderson localization.^{56–58} However in topologically protected systems the conductance plateaus at a constant value of G_0 , manifesting a perfectly conducting channel. Both cases manifest complete dominance of quantum interference over classical conduction processes, and are fueled by Cooperons maintaining quantum coherence.^{59,60}

A second case where Cooperons display loop repetitions is 2-D cylindrical geometries when a magnetic field is parallel to the cylinder. In this geometry the Cooperon produces Altshuler-Aronov-Spivak oscillations where the conductance oscillates as field strength is varied. Without Cooperon loop repetitions the oscillations would have a simple cosine profile. With the loop repetitions the Altshuler-Aronov-Spivak oscillations deviate strongly from a simple cosine signal.^{61,62}

These examples of 1-D systems and 2-D cylindrical systems both prove that Cooperons can display loop repetitions. The remaining question is how Cooperon coherence and loop repetitions are preserved in materials displaying in linear magnetoresistance, which generally have non-cylindrical (simply connected) 3-D or 2-D geometries. At least two avenues are available for protecting Cooperon coherence against scattering. In cer-

tain materials transport may be locally one-dimensional, with carriers constrained along certain race-track like trajectories. This is seen in snake states in graphene, in edge states in the quantum Hall effect, and might also be realized in C_4 symmetry-broken states in underdoped cuprates.^{63–66} When particle motion is locked to a locally one dimensional track, at any particular point the momentum is limited to only two values differing only in sign, and therefore the Cooperon's position and momentum are locked to each other, up to the same sign. Therefore Cooperon coherence is protected in materials where carriers are constrained to move along locally one dimensional tracks.⁶⁷ In conjunction with the fact that linear resistance is a kind of WAL not WL, this scenario suggests that topological physics could play an important role in linear resistance.

A second route to Cooperon coherence is to explicitly invoke strong correlations. For example, there has been much speculation that cuprates and pnictides above the superconducting transition host preformed pairs, precursors of superconducting Cooper pairs which at temperatures above T_c maintain phase coherence up to a length scale λ_ϕ , and which at lower temperatures unite into the superconducting condensate. The phase coherence of these preformed pairs may play a role in protecting the Cooperon's phase coherence at scales similar to λ_ϕ .

Linear magnetoresistance does not require the IR cutoff A_{max} , i.e. the area scale where phase coherence is suppressed, to be very large. For instance, a coherence area of $(100 \text{ \AA})^2$ would allow linear magnetoresistance to extend down to $\approx 0.3\text{T}$.

B. Linear in temperature resistance

We turn to the linear-in-temperature resistance observed in bad metals. As we have seen, the loop area distribution has a smooth logarithmic form with only two characteristic area scales: the UV cutoff A_0 , and the infrared cutoff A_{max} which regulates large loops. The ultraviolet cutoff A_0 may be controlled by many length scales: the scattering length, the lattice spacing, the scale of the Fermi surfaces, and the crossover from WAL to WL which is controlled by the scales at which spin rotation symmetry and time reversal symmetry are broken, etc. These mechanisms depend weakly on temperature.

The main source of temperature dependence comes instead from the infrared cutoff A_{max} which regulates large loops. The tail of the $\ln A$ loop area distribution reflects quantum harmonics where Cooperons repeat the same loop many times, resulting in total areas far larger than the area of a single unrepeatable Cooperon loop. Regardless of which short distance physics controls the loop area distribution of a single Cooperon loop (i.e. without coherence-based repetitions), this physics has no control over the number of loop repetitions, and therefore cannot determine the infrared cutoff A_{max} regulating the loop area distribution. The *only* process available

to supply the cutoff A_{max} on the loop area distribution's tail is quantum decoherence, which is controlled by temperature. In atomic units inverse temperature has units of area, and therefore the decoherence-based cutoff $A_{max} \propto T^{-1}$ scales inversely with temperature. We have already noted this behavior in the specific case of SdH oscillations. This $A_{max} \propto T^{-1}$ scaling is however very robust, both because decoherence is the only process available to regulate the tail of $\ln A$ distribution, and also because the loop areas of the tail are so large that T^{-1} is the only area scale large enough match them.

It is then a simple matter to show that at $B = 0$ the resistance must be linear in temperature. Most simply, the linear magnetoresistance is $R_{xx}(B) = \pi q_C B A_0$. When $B = 0$ the inverse area B^{-1} diverges. The only scale available to take the place of B^{-1} is T^{-1} , and plugging this into the magnetoresistance formula immediately gives linear in temperature resistance $R_{xx}(T) = \pi q_C T A_0$.

Going into more detail, the logarithmic loop area distribution is $G_{xx}(A) \approx -(\pi A_0)^{-1} \ln |A|$. This should be regularized to give positive values because, as we have seen, in WL/WAL the Cooperon does not carry phase information and all Cooperon loop trajectories carry the same weight with the same sign. One possible regularization is to add $(\pi A_0)^{-1} \ln |A_{max}|$. Setting $B = 0$ and integrating with respect to area gives $R_{xx}(B = 0) \approx \pi A_0 / A_{max} \propto \pi A_0 T$ for $A_0 \ll A_{max} \propto T^{-1}$, plus regularization-dependent terms which are sensitive to the cutoffs. When $A_{max} \propto T^{-1}$ is comparable to A_0 the linear dependence on T collapses. At smaller temperatures the linear in temperature resistance is robust because B^{-1} and T^{-1} both act at large length scales and therefore are roughly interchangeable.

C. Coefficients of the linear resistivity

We have shown that quantum coherence and loop repetitions lead to a resistance which scales linearly with both magnetic field and temperature as long as the quantum decoherence area A_{max} is more than both the inverse field $(q_C B)^{-1}$ and the ultraviolet cutoff A_0 . Within our theory the coefficient $\alpha k_B T$ of linear temperature dependence, the coefficient $\beta \mu_B B \approx \beta \mu_B A_{max}^{-1}$ of linear field dependence, and their ratio $\gamma = \alpha / \beta$ are

$$\begin{aligned} \alpha &= \pi A_0 / (A_{max} T) \\ \beta &= \pi q_C \mu_B^{-1} A_0 \\ \gamma &= q_C^{-1} \mu_B / (A_{max} T) \end{aligned} \quad (5)$$

where $\mu_B = 1/2$ and $q_C = 2$ are the Bohr magneton and the Cooperon charge.

Hayes et al measured γ in the high- T_c pnictide superconductor $\text{BaFe}_2(\text{As}_{1-x}\text{P}_x)_2$ at dopings ranging between 0.31 and 0.41, and found that γ was identical to one in atomic units, within their experimental error bar of 7%.¹⁸ Further studies of the cuprate $\text{La}_{2-x}\text{Sr}_x\text{CuO}_4$ and

of $\text{Yb}_{1-x}\text{La}_x\text{Rh}_2\text{Si}_2$ at various dopings near optimal doping have found constants between 0.7 and 2.3.^{18,68} We conclude that γ does depend on the host material, but only mildly, and that it is of order 1.

The value of exactly one for γ is easily explained by combining the Heisenberg uncertainty relation with a $p^2/2m$ dispersion: $B^{-1} = A = \langle (\Delta x)^2 \rangle = \hbar^2 / \langle p^2 \rangle$, where the momentum scale is determined by $\langle p^2 / 2m_C \rangle = T$ and the Cooperon mass is $m_C = 2m_e$. This produces $A_{max} \approx (4T)^{-1}$ and $A_{max} T = 1/4$. The Heisenberg relation used here is a quantum mechanical upper bound on the decoherence scale which can be obtained at a given temperature. These arguments indicate that γ 's physical meaning is simply the effective mass of the charge carriers, i.e. $\gamma = m/m_e$. The experimental observation of $\gamma = 1$, i.e. a $p^2/2m_e$ dispersion, implies that in the compounds studied by Refs.^{18,68} the electrons and holes which contribute to the Cooperon are itinerant carriers with bare electron mass m_e , and are insensitive to the ionic potential of their host material. When $\gamma = 1$ the coefficients α and β of both the linear-in-temperature resistance and the linear magnetoresistance are direct measures of the UV cutoff A_0 , with $R_{xx}(B = 0) = \alpha T \approx \pi A_0 / A_{max}$ and $R_{xx}(B) = \beta \mu_B B \approx 4\pi B A_0$. Where the carrier mass m differs from the bare electron mass m_e , $R_{xx}(B = 0)$ will be multiplied by m/m_e .

As a case in point we determine the UV cutoff A_0 's scaling in several cuprates analyzed by Ref.⁶⁹, which determined the linear coefficient α in $\text{La}_{2-x}\text{Sr}_x\text{CuO}_4$ (LSCO), $\text{YBa}_2\text{Cu}_3\text{O}_{6+\delta}$ (YBCO), $\text{Tl}_2\text{Ba}_2\text{CuO}_{6+\delta}$ (Tl2201), and $\text{HgBa}_2\text{CuO}_{4+\delta}$ (Hg1201). Ref.⁶⁹ found that α is the same in all four compounds if one uses the sheet resistance per CuO_2 plane, not per unit cell. They also found that α is inversely proportional to the doping p for $p \leq 0.20$, where p is the number of holes per unit cell, not per CuO_2 plane. After conversion to atomic units one finds that $\alpha = \pi \times 64 a_0^2 \times p^{-1}$.⁸⁰ We surmise on dimensional grounds that α should not depend on the doping, but instead on the 2-D carrier density ρ_{2D} . Using $p = \rho_{2D} \times \mathcal{A}$ where $\mathcal{A} \approx 53a_0^2$ is the cross-section of the unit cell in the cuprates' copper oxide plane, we arrive at $R_{xx}(B = 0) = 0.30 \times \pi \times (\rho_{2D} A_{max})^{-1}$ and $R_{xx}(B) = 0.30 \times \pi \times 4\mu_B \times \rho_{2D}^{-1} B$, where $A_{max} = (4T)^{-1}$. This suggests that in these compounds the UV cutoff A_0 of the loop area distribution is the inverse of the carrier density, i.e. $A_0 = \rho_{2D}^{-1}$, and that the resistance includes a dimensionless normalization factor $\mathcal{N} = 0.30 \times \pi$. This normalization factor \mathcal{N} may reflect details of the Cooperon coherence mechanism and the UV and IR cutoffs. It also reflects the loop area distribution prior to coherence-induced repetitions, where we chose the most obvious normalization: 1 in atomic units, resulting in $\mathcal{N} = \pi$. Rounding the experimentally determined normalization factor $\mathcal{N} = 0.30 \times \pi$ to 1, with a 6% difference that is close to Ref.⁶⁹'s experimental error, obtains $R_{xx}(T) = (A_{max} \rho_{2D})^{-1}$ and $R_{xx}(B) = 4\mu_B \times \rho_{2D}^{-1} B$, where $A_{max} = (4T)^{-1}$.⁸¹ These formulas offer the possibility of determining the charge carrier density directly

from either the linear magnetoresistance or the linear in temperature resistance, without any speculation about the compound's chemistry or band structure.

D. The weak-field and small-temperature regimes

These two regimes are distinct. Time reversal symmetry, combined with the presence of a fairly sharp (faster than power law) infrared cutoff A_{max} , requires a B^2 behavior at small fields, i.e. $\rho = \rho_0 + (B/B_0)^2$. This was found in Ref.¹⁸ and confirmed by Ref.⁶⁸.

In particular, Ref.¹⁸ verified that $\rho = \rho_0 + (\mu_B B/T)^2/2$ in $\text{BaFe}_2(\text{As}_{1-x}\text{P}_x)_2$ and found a smooth form which interpolates between small and large fields: $\rho_0 + \sqrt{\mu_B^2 B^2 + T^2}$. While this form includes the correct small B limit with T fixed, it gives only one form out of many possible forms for the small T limit with B fixed. The small T behavior is sensitive to the tail of the loop area distribution $G_{xx}(A)$, because finite B does not impose a sharp cutoff on the integral $G_{xx}(B) = \int dA \exp(iAB)G_{xx}(A)$. In point of fact Ref.¹⁸ saw a quadratic form in $\text{BaFe}_2(\text{As}_{1-x}\text{P}_x)_2$ while Ref.⁶⁸ saw a linear form in $\text{La}_{2-x}\text{Sr}_x\text{CuO}_4$.

Systematic studies of the tail of $G_{xx}(A)$ throughout the high- T_c phase diagram are likely to be very illuminating. Such studies require only an increased attention to the magnetoconductance's sensitivity to small changes in B . Detailed studies at high resolution in B will reveal the form of the IR cutoff. In particular, any sharp cutoff (faster than power law) at A_{max} will manifest in the magnetoconductance as fast ripples which will be visible even at large fields. The ripples will be superimposed on the linear signal, with a profile qualitatively similar to that seen in Ref.¹. Considering for example a sharp IR cutoff at $A_{max} = (4T)^{-1}$, at $T = 0.1\text{K}$ the ripple period $2\pi/A_{max}$ will be 1.87 Tesla.

IV. FINAL COMMENTS

We have suggested that the bad metals' linear resistance is caused by interaction-induced scattering. In principle the scattering could be caused by anything that fluctuates at a time scale longer than the time τ required to go around a loop. Using $T^{-1} = 4A$ from section III C and $\tau = \hbar/k_B T$, we find that τ is three picoseconds for loops of area $A = (100 \text{\AA})^2$.

If the scattering source were truly static, for instance in topological insulators displaying linear resistance, then Universal Conductance Fluctuations should be seen in the magnetoconductance, and possibly individual phase coherent loops would be visible to STM experiments. We expect that in bad metals the scattering is caused not by static impurities but by interactions, so that UCFs will average to zero. In fact UCFs have not been reported in bad metals, although very few studies of the bad metals'

magnetoconductance have been performed. If UCFs cannot be found in bad metals, this would indicate that scattering is indeed caused by time dependent fluctuations, like the fluctuating and glassy signals that have been observed in Refs.^{70,71} using transport measurements and in Refs.^{72,73} using muon spin relaxation.

It is also worthwhile to point out that, if it is true that the linear magnetoresistance is caused by Cooperons and that the scattering source fluctuates with time, then magnetoresistance experiments on small nanorings fabricated from linear magnetoresistance materials and bad metals should observe that the carriers have charge $q_C = 2q_e$. In other words, Aharonov-Bohm oscillations will average to zero at the same time scale at which the scattering source fluctuates, while Altshuler-Aronov-Spivak oscillations will remain because they are robust against scattering.

Lastly we point out that, in our view, one of the most important aspects of the present work is its methodology, which focuses on geometric analysis of electron and hole loops, and especially on the loop area distribution that can be obtained from Fourier transforms of magnetoconductance data. We have presented a non-perturbative framework for understanding electron and hole behavior that is completely independent of any assumptions about Fermi liquid physics and gives additional physical insight. We anticipate experiments focusing on the loop area distribution, with special attention to accessing large areas using carefully controlled small increments of the field, to removing leads effects, and to performing careful Fourier transforms. We also expect increased use of vector magnets and multi-dimensional Fourier transforms.

Appendix A: Alternate Regularizations.

We demonstrate in this supporting information that reasonable regularizations of the Fourier transform of x^{-1} produce a logarithm, and vice versa. In our first example we perform the Fourier transform of x^{-1} .

$$\begin{aligned} \mathcal{A}(\gamma, x_0, k) &= \int_0^\infty dx \cos(kx) \exp(-\gamma x) \frac{1}{x + x_0} \\ &= \text{Re}(\exp(x_0(\gamma + ik)) \Gamma(0, x_0(\gamma + ik))) \end{aligned} \quad (\text{A}1)$$

$\mathcal{A}(\gamma = 0, x_0 = 1, k)$ is approximately logarithmic in the range $x = [0, 0.1] \times 2\pi$, as can be verified by plotting $\mathcal{A}(\gamma = 0, x_0 = 1, k) / \log(k)$.

Our second example again performs the Fourier transform of x^{-1} , but with a different UV cutoff.

$$\mathcal{B}(\gamma, x_0, k) = \int_0^\infty dx \cos(kx) \exp(-\gamma x) \frac{1}{\sqrt{1 + x^2/x_0^2}} \quad (\text{A}2)$$

$\mathcal{B}(\gamma, x_0, k)$ can be integrated exactly, and includes Bessel, logarithmic, Struve, and hypergeometric functions. $\mathcal{B}(\gamma = 0, x_0 = 1, k)$ is approximately logarithmic in the range $x = [0, 0.1] \times 2\pi$.

Our third example performs the Fourier transform of $\log|x|$.

$$\mathcal{C}(\gamma, x_0, k, \nu) = \int_0^\infty dx \cos(kx) \exp(-\gamma x) \log|1 + (x/k)^\nu|$$

This integral can be performed analytically for many values of $\nu = 1, 3/2, 5/3, 7/4, 19/10, 2$, and is always proportional to k^{-1} plus corrections of order k at small k in the range $[0, 0.2]$. For $\nu = 3/2, 5/3, 7/4, 19/10$ it is written in terms of Meijer functions. The value of $k \times \mathcal{C}(\gamma = 0, x_0 = 1, k, \nu)$ at $k = 0$ is generally a rational fraction times π . For instance,

$$\begin{aligned} \mathcal{C}(\gamma, x_0, k, \nu = 1) &= \text{Re}(\omega^{-1} \exp(\omega x_0) \Gamma(0, \omega x_0)) \\ \omega &= -ik + \gamma. \end{aligned} \quad (\text{A4})$$

Acknowledgments

We gratefully acknowledge formative and stimulating discussions with S. Kettemann, A. Leggett, Y. Li, C. Lin, X. Dai, V. Dobrosavljevic, H.-J. Lee, Q. Wu, T. Ohtsuki, J. Zaanen, K. Schalm, T. Takimoto, K.-S. Kim, X. Wan, P. Niklowitz, A. Ho, J. Saunders, L. Levitin, J. Koelzer, T. Schapers, H. Luth, C. Weyrich, P. Hasnip, A. Kim, M. Ma, P. Coleman, S. Hayden, I. Bozovic, P. Abbamonte, and G. Parisi. We also thank especially A. Petrovic who discussed the manuscript during preparation. **Funding:** We acknowledge support from EPSRC grant EP/M011038/1.

^{*} Electronic address: vincent@sacksteder.com

- ¹ S. X. Zhang, R. D. McDonald, A. Shekhter, Z. X. Bi, Y. Li, Q. X. Jia, and S. T. Picraux, *Applied Physics Letters* **101**, 202403 (2012).
- ² W. Zhang, R. Yu, W. Feng, Y. Yao, H. Weng, X. Dai, and Z. Fang, *Phys. Rev. Lett.* **106**, 156808 (2011).
- ³ X. Wang, Y. Du, S. Dou, and C. Zhang, *Phys. Rev. Lett.* **108**, 266806 (2012).
- ⁴ J. Feng, Y. Pang, D. Wu, Z. Wang, H. Weng, J. Li, X. Dai, Z. Fang, Y. Shi, and L. Lu, *Phys. Rev. B* **92**, 081306 (2015).
- ⁵ F. Kisslinger, C. Ott, C. Heide, E. Kampert, B. Butz, E. Specker, S. Shallcross, and H. B. Weber, *Nature Physics* **11**, 650 (2015).
- ⁶ C. Zhang, C. Guo, H. Lu, X. Zhang, Z. Yuan, Z. Lin, J. Wang, and S. Jia, *Phys. Rev. B* **92**, 041203 (2015).
- ⁷ K. Wang, D. Graf, and C. Petrovic, *Phys. Rev. B* **89**, 125202 (2014).
- ⁸ X. Xu, W. H. Jiao, N. Zhou, Y. Guo, Y. K. Li, J. Dai, Z. Q. Lin, Y. J. Liu, Z. Zhu, X. Lu, et al., *Journal of Physics: Condensed Matter* **27**, 335701 (2015).
- ⁹ Y. Sun, S. Pyon, and T. Tamegai, *Phys. Rev. B* **93**, 104502 (2016).
- ¹⁰ Y. Tanabe, K. K. Huynh, S. Heguri, G. Mu, T. Urata, J. Xu, R. Nouchi, N. Mitoma, and K. Tanigaki, *Phys. Rev. B* **84**, 100508 (2011).
- ¹¹ D. Bhoi, P. Mandal, P. Choudhury, S. Pandya, and V. Ganesan, *Applied Physics Letters* **98**, 172105 (2011).
- ¹² J. Fenton and A. J. Schofield, *Phys. Rev. Lett.* **95**, 247201 (2005).
- ¹³ A. E. Koshelev, *Phys. Rev. B* **88**, 060412 (2013).
- ¹⁴ A. A. Abrikosov, *Phys. Rev. B* **58**, 2788 (1998).
- ¹⁵ T. Khouri, U. Zeitler, C. Reichl, W. Wegscheider, N. E. Hussey, S. Wiedmann, and J. C. Maan, *Phys. Rev. Lett.* **117**, 256601 (2016).
- ¹⁶ M. M. Parish and P. B. Littlewood, *Nature* **426**, 162 (2003).
- ¹⁷ N. E. Hussey, K. Takenaka, and H. Takagi, *Philosophical Magazine* **84**, 2847 (2004).
- ¹⁸ I. M. Hayes, R. D. McDonald, N. P. Breznay, T. Helm, P. J. Moll, M. Wartenbe, A. Shekhter, and J. G. Analytis, *Nature Physics* **12**, 916 (2016).
- ¹⁹ P. Giraldo-Gallo, J. Galvis, Z. Stegen, K. Modic, F. Balakirev, J. Betts, X. Lian, C. Moir, S. Riggs, J. Wu, et al., *Science* **361**, 479 (2018).
- ²⁰ R. Kumar, S. Singh, and S. Nair, arXiv preprint arXiv:1801.03768 (2018).
- ²¹ R. P. Feynman and A. R. Hibbs, *Quantum mechanics and path integrals* (McGraw-Hill, 1965).
- ²² S. Hikami, A. I. Larkin, and Y. Nagaoka, *Progress of Theoretical Physics* **63**, 707 (1980).
- ²³ K. Efetov, *Supersymmetry in disorder and chaos* (Cambridge University Press, 1999).
- ²⁴ J. Rammer, *Quantum transport theory* (CRC Press, 2018).
- ²⁵ L. Schäfer and F. Wegner, *Zeitschrift für Physik B Condensed Matter* **38**, 113 (1980).
- ²⁶ S. A. Hartnoll, *Nature Physics* **11**, 54 (2015).
- ²⁷ N. Nagaosa and P. A. Lee, *Phys. Rev. Lett.* **64**, 2450 (1990).
- ²⁸ C. M. Varma, P. B. Littlewood, S. Schmitt-Rink, E. Abrahams, and A. E. Ruckenstein, *Phys. Rev. Lett.* **63**, 1996 (1989), URL <https://link.aps.org/doi/10.1103/PhysRevLett.63.1996>.
- ²⁹ R. A. Davison, K. Schalm, and J. Zaanen, *Phys. Rev. B* **89**, 245116 (2014), URL <https://link.aps.org/doi/10.1103/PhysRevB.89.245116>.
- ³⁰ A. A. Patel, J. McGreevy, D. P. Arovas, and S. Sachdev, *Phys. Rev. X* **8**, 021049 (2018), URL <https://link.aps.org/doi/10.1103/PhysRevX.8.021049>.
- ³¹ G. Bergman, *Phys. Rev. Lett.* **48**, 1046 (1982), URL <https://link.aps.org/doi/10.1103/PhysRevLett.48.1046>.
- ³² K. G. Wilson, *Phys. Rev. D* **10**, 2445 (1974).
- ³³ R. P. Feynman, *Phys. Rev.* **80**, 440 (1950).
- ³⁴ A. Ashtekar and C. Rovelli, *Classical and Quantum Gravity* **9**, 1121 (1992).
- ³⁵ L. Onsager, *The London, Edinburgh, and Dublin Philosophical Magazine and Journal of Science* **43**, 1006 (1952).
- ³⁶ B. Laikhtman and E. L. Altshuler, *Annals of Physics* **232**, 332 (1994).
- ³⁷ B. L. Altshuler and A. G. Aronov, *JETP Lett.*, **33**, 499 (1981).
- ³⁸ V. K. Dugaev and D. E. Khmelnitskii, *Sov. Phys. JETP* **59**, 1038 (1984).
- ³⁹ G. Bergmann, *Phys. Rev. B* **39**, 11280 (1989).
- ⁴⁰ O. E. Raichev and P. Vasilopoulos, *Journal of Physics:*

Condensed Matter **12**, 589 (2000).

⁴¹ J. S. Meyer, A. Altland, and B. L. Altshuler, Phys. Rev. Lett. **89**, 206601 (2002).

⁴² I. Garate and L. Glazman, Phys. Rev. B **86**, 035422 (2012).

⁴³ C. W. J. Beenakker and H. van Houten, Phys. Rev. B **38**, 3232 (1988).

⁴⁴ C. J. Lin, X. Y. He, J. Liao, X. X. Wang, V. S. IV, W. M. Yang, T. Guan, Q. M. Zhang, L. Gu, G. Y. Zhang, et al., Phys. Rev. B **88**, 041307 (2013).

⁴⁵ V. E. Sacksteder, K. B. Arnardottir, S. Kettemann, and I. A. Shelykh, Phys. Rev. B **90**, 235148 (2014).

⁴⁶ Q. Wu and V. E. Sacksteder, Phys. Rev. B **90**, 045408 (2014).

⁴⁷ K. Nomura, M. Koshino, and S. Ryu, Phys. Rev. Lett. **99**, 146806 (2007).

⁴⁸ J. H. Bardarson, J. Tworzydło, P. W. Brouwer, and C. W. J. Beenakker, Phys. Rev. Lett. **99**, 106801 (2007).

⁴⁹ C. H. Lewenkopf, E. R. Mucciolo, and A. H. Castro Neto, Phys. Rev. B **77**, 081410 (2008).

⁵⁰ G. M. Minkov, A. V. Germanenko, V. A. Larionova, S. A. Negashov, and I. V. Gornyi, Phys. Rev. B **61**, 13164 (2000), URL <https://link.aps.org/doi/10.1103/PhysRevB.61.13164>.

⁵¹ D. V. Baxter, R. Richter, M. L. Trudeau, R. W. Cochrane, and J. O. Strom-Olsen, Journal de Physique **50**, 1673 (1989).

⁵² A. P. Dmitriev, V. Y. Kachorovskii, and I. V. Gornyi, Phys. Rev. B **56**, 9910 (1997), URL <https://link.aps.org/doi/10.1103/PhysRevB.56.9910>.

⁵³ V. Gasparyan and A. Y. Zyuzin, Sov. Phys. Solid State **27**, 999 (1985).

⁵⁴ M. Dyakonov, Solid state communications **92**, 711 (1994).

⁵⁵ A. Cassam-Chenai and B. Shapiro, Journal de Physique I **4**, 1527 (1994).

⁵⁶ K. Ishii, Progress of Theoretical Physics Supplement **53**, 77 (1973).

⁵⁷ B. Simon and T. Spencer, Communications in Mathematical Physics **125**, 113 (1989).

⁵⁸ C. W. J. Beenakker, Rev. Mod. Phys. **69**, 731 (1997), URL <https://link.aps.org/doi/10.1103/RevModPhys.69.731>.

⁵⁹ T. Ando and H. Suzuura, Journal of the Physical Society of Japan **71**, 2753 (2002).

⁶⁰ Y. Takane, Journal of the Physical Society of Japan **73**, 1430 (2004).

⁶¹ B. L. Altshuler, A. G. Aronov, and B. Z. Spivak, JETP Lett. **33**, 94 (1981).

⁶² V. E. Sacksteder and Q. Wu, Phys. Rev. B **94**, 205424 (2016).

⁶³ L. Oroszlány, P. Rakyta, A. Kormányos, C. J. Lambert, and J. Cserti, Phys. Rev. B **77**, 081403 (2008).

⁶⁴ T. K. Ghosh, A. De Martino, W. Häusler, L. Dell'Anna, and R. Egger, Phys. Rev. B **77**, 081404 (2008).

⁶⁵ J. R. Williams and C. M. Marcus, Phys. Rev. Lett. **107**, 046602 (2011).

⁶⁶ K. Fujita, C. K. Kim, I. Lee, J. Lee, M. H. Hamidian, I. A. Firsov, S. Mukhopadhyay, H. Eisaki, S. Uchida, M. J. Lawler, et al., Science **344**, 612 (2014).

⁶⁷ Q. Wu, L. Du, and V. E. Sacksteder, Phys. Rev. B **88**, 045429 (2013).

⁶⁸ P. Giraldo-Gallo, J. A. Galvis, Z. Stegen, K. A. Modic, F. F. Balakirev, J. B. Betts, X. Lian, C. Moir, S. C. Riggs, J. Wu, et al., arXiv preprint arXiv:1705.05806 (2017).

⁶⁹ N. Barišić, M. K. Chan, Y. Li, G. Yu, X. Zhao, M. Dressel, A. Smontara, and M. Greven, Proceedings of the National Academy of Sciences **110**, 12235 (2013).

⁷⁰ I. Raičević, J. Jaroszyński, D. Popović, C. Panagopoulos, and T. Sasagawa, Phys. Rev. Lett. **101**, 177004 (2008).

⁷¹ G. R. Jelbert, T. Sasagawa, J. D. Fletcher, T. Park, J. D. Thompson, and C. Panagopoulos, Phys. Rev. B **78**, 132513 (2008).

⁷² C. Panagopoulos, A. P. Petrovic, A. D. Hillier, J. L. Tallon, C. A. Scott, and B. D. Rainford, Phys. Rev. B **69**, 144510 (2004).

⁷³ J. Zhang, Z. Ding, C. Tan, K. Huang, O. O. Bernal, P.-C. Ho, G. D. Morris, A. D. Hillier, P. K. Biswas, S. P. Cottrell, et al., Science Advances **4**, eaao5235 (2018).

⁷⁴ G. P. Mikitik and Y. V. Sharlai, Phys. Rev. Lett. **82**, 2147 (1999).

⁷⁵ A. J. Leggett, *Quantum liquids: Bose condensation and Cooper pairing in condensed-matter systems* (Oxford University Press, 2006).

⁷⁶ T. Hu, Y. Liu, H. Xiao, G. Mu, and Y.-f. Yang, Scientific reports **7**, 9469 (2017).

⁷⁷ A slightly different result $\cos(A/NA^F)$ obtains for the N -th Landau level of Dirac fermions.⁷⁴

⁷⁸ To verify that loop area distribution for Landau levels and SdH oscillations decays exponentially, we numerically Fourier transformed the conductance formulas in Ref.³⁶, because analytical formulas for the Fourier transform of this signal are not available.

⁷⁹ At very strong magnetic fields, when the magnetic length $\sqrt{\hbar c/eB}$ is compared with the mean free path, there is a further transition to $G_{xx} \propto 1/\sqrt{B}$ behavior.^{52–55}

⁸⁰ Up to the multiplicative constant, this formula $R \propto T/p$ is the same as Ref.²⁷'s RVB result. See also Ref.⁷⁵ for discussion of the resistance per CuO₂ plane.

⁸¹ Ref.⁷⁶ has argued that the linear coefficient of the resistivity dR/dT is proportional to λ_L^2 across a range of cuprate, pnictide, and heavy fermion materials, where λ_L is the London penetration depth. Since both Ref.⁷⁶ and Ref.⁶⁹ analyze the same data on LSCO, this suggests a scaling relationship between λ_L^2 and the inverse carrier density ρ_{2D}^{-1} .